**Climate
of the Past**

Vegetation-climate interactions in the warm mid-Cretaceous

J. Zhou[1]**, C. J. Poulsen**[1]**, N. Rosenbloom**[2]**, C. Shields**[2]**, and B. Briegleb**[2]

[1]Department of Earth and Environmental Sciences, University of Michigan, USA
[2]National Center for Atmospheric Research, Boulder, Colorado, USA

Correspondence to: J. Zhou (zotsing@umich.edu)

Abstract. Vegetation-climate interactions are thought to have amplified polar warmth during past warm periods. Here, we explore the vegetation-climate interactions in the mid-Cretaceous using a fully coupled ocean-atmosphere general circulation model with a dynamic vegetation component. We run simulations with 1x, 10x and 16x pre-industrial atmospheric CO_2. Results show that forests expand from mid-latitudes to high latitudes as CO_2 increases from 1x to 10x and 16x, mainly due to the CO_2-induced warming. This expansion of mid-to-high latitude forests are largely supported by the distribution of mid-Cretaceous fossil woods and coal deposits. Globally, the presence of vegetation increases mean annual temperature and precipitation by 0.9 °C and 0.11 mm day^{-1} relative to bare ground. High-latitude warming induced by the presence of vegetation (∼1.9 °C) is less than half of that reported in previous studies. The weaker warming here is mainly due to less pronounced albedo feedbacks, and to a less extent, reduced poleward heat transport via weakening of the meridional overturning circulation. Our results suggest that other mechanisms in addition to high atmospheric CO_2 and high-latitude vegetation are required to maintain the polar warmth.

1 Introduction

The mid-Cretaceous (∼100 Ma) was a period of extreme polar warmth. Paleoclimate proxies indicate that mean annual temperature were as high as 20 °C and 13 °C over polar ocean and land (Bice et al., 2003; Jenkyns et al., 2004; Spicer et al., 2002, 2008). The cause of global warmth is widely accepted to be caused by high atmospheric CO_2 levels (Barron and Washington, 1985) resulting from volcanic outgassing.

However, simulations of Cretaceous climate using general circulation models (GCMs) with high atmospheric CO_2 predict polar temperatures that are too cool (Barron et al., 1995; Poulsen et al., 1999, 2004; Spicer et al., 2008) challenging our understanding of greenhouse climate.

Several hypotheses have been proposed to reconcile this high-latitude model-data discrepancy including enhanced poleward heat transport via strengthening of atmospheric or oceanic circulation (e.g., Covey and Barron, 1988; Farrel, 1990; Korty et al., 2008), increased local radiative forcing through high-latitude cloud feedbacks (e.g., Abbot and Tziperman, 2008; Sloan and Pollard, 1998; Kump and Pollard, 2008), high atmospheric methane levels (Bice et al., 2006) and high-latitude forests (Deconto et al., 2000; Otto-Bliesner and Upchurch, 1997; Upchurch et al., 1998). Of these mechanisms only the existence of high-latitude forests is directly supported by observations in the geological records (e.g., Herman and Spicer, 1996; Falcon-Lang et al., 2001; Spicer and Parrish, 1986; Spicer et al., 1993).

Previous studies have reported that the expansion of forests into polar regions in the Late Cretaceous may have warmed high-latitude regions by 4–7 °C (Deconto et al., 2000; Otto-Bliesner and Upchurch, 1997; Upchurch et al., 1998). The warming is mainly attributed to a reduction in surface albedo due to the masking of snow via forests and melting of sea ice via transfer of heat from vegetated land to ocean. The role of vegetation feedbacks on polar warming has not been examined for the mid-Cretaceous when CO_2 levels were thought to have been higher. In addition, previous Late Cretaceous modelling studies coupled atmospheric general circulation models (AGCMs) to mixed-layer ocean models that do not allow for dynamic ocean feedbacks. Paleoclimate modelling of Cenozoic intervals

has demonstrated that vegetation-induced climate change can influence the strength of the ocean meridional overturning circulation (MOC) (Brovkin, 2002; Brovkin et al., 2009; Ganopolski et al., 1998; Lohmann et al., 2006). Of possible relevance to Cretaceous polar warmth, Lohmann et al. (2006) report that the prescribed present to warm late-Miocene vegetation changes strengthen the North Atlantic MOC by more than 3 times, leading to a warming over the mid-to-high latitude North Atlantic by up to 8 °C. Furthermore, previous studies investigated the Cretaceous vegetation-climate interactions using prescribed vegetation changes (Otto-Bliesner and Upchurch, 1997; Upchurch et al., 1998) or an equilibrium vegetation model (Deconto et al., 2000), which do not allow realistic transient climate-vegetation interactions as in dynamic global vegetation models (Peng, 2000).

In view of the limitations of these earlier studies, we re-examine the vegetation-climate interactions in the Cretaceous under high atmospheric CO_2 using a fully coupled ocean-atmosphere GCM with a dynamic vegetation component (CCSM3). This study addresses two main questions: (1) Can CCSM3 simulate the mid-Cretaceous vegetation distribution, and if so, at what atmospheric CO_2 levels? (2) How does the simulated vegetation affect mid-Cretaceous climate? We first examine the climate control on vegetation by comparing the vegetation pattern with low (1x) and high (10x and 16x) atmospheric CO_2. We then investigate the impact of vegetation on climate by comparing a simulation with the maximum simulated vegetation mass to a simulation without vegetation.

2　Methods

Cretaceous simulations were completed with NCAR's Community Climate System Model version 3 (CCSM3), a fully coupled GCM with dynamic global vegetation (Collins et al., 2006; Levis et al., 2004). CCSM3 was run in a T31x3 configuration, with a T31 spectral truncation ($3.75° \times 3.75°$), 26-level atmosphere component model (Community Atmospheric Model) coupled to a nominal 3° (~400 km in the zonal direction at the equator), 25-level ocean component model (Parallel Ocean Program). To increase grid cell density around the Arctic area and promote interbasin exchange, the grid North pole is displaced to 75° N, 120° E in our simulations. The land surface model (Community Land Model) and dynamic global vegetation model (CLM-DGVM) are set to the same horizontal resolution as atmosphere; the sea ice component model (Community Sea Ice Model) has the same horizontal resolution as the ocean. The simulated present-day climate with this low-resolution configuration is comparable to the higher-resolution (i.e., T42x1 and T85x1) results and modern observation (Yeager et al., 2006). Due to its relatively low computational cost, this economical configuration is considered a good approach for paleoclimate studies (e.g., Kiehl and Shields, 2005).

Vegetation distribution in CLM-DGVM is largely determined by solar radiation, air temperature, soil moisture and atmospheric CO_2 concentration (Bonan and Levis, 2006). For example, the survival and establishment of vegetation are constrained by bioclimatic parameters including monthly air temperature, growing degree days (GDD) and mean annual precipitation (Table 1). CLM-DGVM classifies vegetation as patches of plant function types (PFTs) (Levis et al., 2004). A PFT represents the average individual for a group of species that share similar physiological and morphological characteristics. All PFTs can co-exist in a grid cell's soil-covered portion when climate allows. CLM-DGVM calculates vegetation dynamics including allocation, biomass turnover, mortality, aboveground competition, fire and establishment yearly. Levis et al. (2004) provide a detailed description of vegetation dynamics. Vegetation biogeography and structure is also updated yearly. Canopy phenology is updated daily. The communication between CLM-DGVM and the atmosphere model is achieved through exchanges of energy, momentum, and moisture every 20 min (Levis et al., 2004). Our version of CLM-DGVM does not simulate transient changes in atmospheric CO_2.

Eight PFTs are defined in this study, with one herbaceous PFT (C_3 grasses) and seven woody PFTs (trees) (Table 1). We exclude C_4 grasses in this study because C_4 grasses did not become ecologically important until the Early-middle Miocene (Cerling et al., 1993; Jacobs et al., 1999). Though the origin of C_3 grassland is no earlier than the Late Cretaceous (Jacobs et al., 1999), we include C_3 grasses for two reasons: (1) CLM-DGVM does not have a PFT representing shrubs, therefore, shrublands are often simulated as desert or grasslands (Bonan et al., 2003); and (2) the fossil record suggested a widespread distribution of herbaceous vegetation during the mid-Cretaceous (Spicer et al., 1993).

To determine the equilibrium vegetation distribution corresponding to the mid-Cretaceous warm climate, we conducted three simulations implementing CLM-DGVM, namely, 1xDGVM, 10xDGVM and 16xDGVM (Table 2). An additional experiment (10xBG) was run with land surface prescribed as bare ground. Atmospheric CO_2 concentration was set to 1x, 10x or 16x pre-industrial levels. 16x pre-industrial levels CO_2 likely falls in the upper limit of the estimated mid-Cretaceous atmospheric CO_2 levels (see summary in Bice and Norris, 2002). DGVM simulates physiological changes in photosynthesis and stomatal conductance due to changes in the ambient partial pressure of CO_2. However, in these simulations, we used the default physiological pCO_2 (355 ppmv) for three reasons: (1) modern studies show that high pCO_2 does not necessarily enhance plant productivity (e.g., Körner, 2003). Nutrients (e.g., nitrogen and phosphorus) appear to become a limiting factor for photosynthesis with increasing pCO_2. (2) CO_2 physiological effects likely vary significantly from species to species. Whether the modern empirical equation is applicable to ancient plants is questionable. And, (3) our sensitivity test shows that the

Table 1. Bioclimatic parameters for survival and establishment of plant functional type (PFT). Adapted from Table 1 in Bonan et al. (2003).

PFT	$T_{c,min}$ (°C)	$T_{c,max}$ (°C)	T_{hs} (°C)	GDD (°C day)	P (mm yr^{-1})
Tropical broadleaf evergreen	15.5	NA	NA	NA	100
Tropical broadleaf deciduous	15.5	NA	NA	NA	100
Temperate needleleaf evergreen	−2.0	22.0	NA	900	100
Temperate broadleaf evergreen	3.0	18.8	NA	1200	100
Temperate broadleaf deciduous	−17.0	15.5	NA	1200	100
Boreal needleleaf evergreen	−32.5	−2.0	23	600	100
Boreal deciduous	NA	−2.0	23	350	100
C_3 grasses	−17.0	NA	NA	0	100

All values are based on 20-yr running mean. $T_{c,min}$ = coldest minimum monthly air temperature for survival, $T_{c,max}$ = warmest minimum monthly air temperature for establishment, T_{hs} = heat stress air temperature for survival, GDD_{min} = minimum annual growing degree-days above 5 °C, which is the sum of all positive values of difference between average daily temperature and 5 °C in one year, P_{min} = minimum annual precipitation for establishment. The only difference between our defined PFTs and the ones in Bonan et al. (2003) is our treatment of $T_{c,max}$ for C_3 grasses, to allow C_3 grasses to expand over the C_4 grass range, we eliminate the maximum temperature threshold for C_3 grasses.

model cannot handle physiological pCO$_2$ as high as 10x/16x pre-industrial levels. All experiments were run with a reduced solar constant (99 % of modern) (Gough, 1981) and present day orbital parameters. The model geography and topography were based on mid-Cretaceous (100 Ma) reconstructions from PALEOMAP project (Scotese, 2001). Because sea level was at highstand, global land area is 18.6 % less than present day. Following Poulsen et al. (2003), we applied an age-depth relationship to reconstruct bathymetry for the deep ocean regions with known magnetic lineations (Barron, 1987). Elsewhere, deep-ocean depths were set to 5300 m. River runoff is routed to the ocean via a river transport model (Branstetter, 2001). All experiments were initiated using zonal ocean temperatures and salinity from a warm Late Cretaceous simulation (Otto-Bliesner et al., 2002). Vegetation was initialized from a 300 yr integration of a Cretaceous CAM3-DGVM simulation with 10x pre-industrial CO$_2$ levels. Levis et al. (2004) report that global vegetation distribution approaches equilibrium in a few hundred years in CLM-DGVM. Each of our Cretaceous experiments was run in excess of 1600 yr (Table 2). The changes of global vegetated land cover fraction are statistically insignificant (∼0.1 % century^{-1}) by the end of simulations. The drifts in simulated global mean ocean temperature over the last 200 yr are also small (on the order of 0.1 °C century^{-1}) for all experiments.

3 Results

3.1 Response of vegetation to CO$_2$ levels

3.1.1 Simulated surface temperature and precipitation

The increase of atmospheric CO$_2$ leads to an increase in global annual mean surface temperature from 13.6 to 24.0 and 25.6 °C in the 1xDGVM, 10xDGVM and 16xDGVM experiments, respectively (Table 2). Continental surface tem-
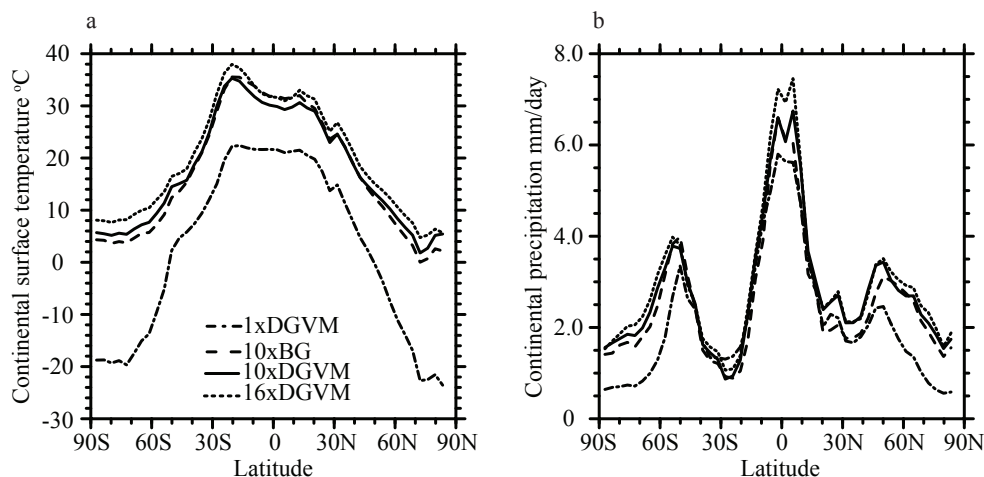
peratures increase by up to ∼10 °C at low latitudes and 29 °C at high latitudes as a result of increasing CO$_2$ from 1 to 16x PAL (Fig. 1a). Consistent with the increase in surface temperature, global annual mean precipitation increases from 2.90 mm day^{-1} in the 1xDGVM experiment to 3.47 and 3.56 mm day^{-1} in the 10xDGVM and 16xDGVM experiments (Table 2). The increase in continental precipitation between 1xDGVM and 16xDGVM experiments is up to 1.8 (∼33 %) and 1.9 (∼150 %) mm day^{-1} at low and mid-to-high latitudes. In contrast, the continental precipitation decreases by ∼0.3 mm day^{-1} (∼20 %) in the southern subtropical latitudes (∼20–30° S) (Fig. 1b).

3.1.2 Simulated global vegetation distribution

In the 1xDGVM experiment, the tropics, subtropics, mid-latitudes and high latitudes are dominated by evergreen trees, grasses, mixture of evergreen and deciduous trees and polar desert, respectively (Fig. 2a–c). In the high CO$_2$ experiments, trees (especially deciduous) and grasses advance into the northern high latitudes and Antarctica (Fig. 2d–i). In the northern high latitudes (60–90° N), average fractional tree cover over the soil-covered land increases from 0.7 % in the 1xDGVM experiment to 61 % (10xDGVM) and 59 % (16xDGVM). The change in tree cover at the southern high latitudes (60–90° S) is slightly less than the northern high latitudes, increasing from 4 % (1xDGVM) to 51 % (10xDGVM) and 43 % (16xDGVM). In contrast, tree cover at low latitudes (30° S–30° N) decreases from 60 % (1xDGVM) to 54 % (10xDGVM) and 50 % (16xDGVM). As a result of the poleward expansion of trees and grasses, area-weighted global vegetation cover increases from 56 % (1xDGVM) to 85 % (10xDGVM and 16xDGVM). Global net primary production (NPP), which is equal to the net gain of carbon through photosynthesis and respiration, is estimated to be 61.8 PgC yr^{-1} in the 1xDGVM experiment, comparable to observational estimates of present-day NPP (Schlesinger, 1997). Due to the increase in global vegetation

Table 2. Mid-Cretaceous CCSM3 experiments and global annual mean surface temperature (SAT) and precipitation.

Experiment	Atm. CO_2 (ppmv)	Vegetation	Integration (year)	SAT (°C)	Precipitation (mm day^{-1})
1xDGVM	280	DGVM	2125	13.6	2.90
10xBG	2800	Bare ground	1626	23.1	3.36
10xDGVM	2800	DGVM	1637	24.0	3.47
16xDGVM	4480	DGVM	1615	25.6	3.56

Fig. 1. Zonal-average annual mean continental surface temperature (°C) **(a)**; and precipitation (mm day^{-1}) **(b)** for the 1xDGVM (black dash-dot line), 10xBG (black dashed line), 10xDGVM (black solid line) and 16xDGVM (black dotted line) experiments, respectively.

cover, NPP increases by 13.5 PgC yr^{-1} (21.8 %) in the 10xDGVM experiment and 10.9 PgC yr^{-1} (17.6 %) in the 16xDGVM experiment relative to the 1xDGVM experiment.

The large-scale changes in vegetation distribution are linked to changes in surface temperatures and precipitation. The expansion of trees and grasses at mid- and high latitudes in the two high CO_2 experiments is mainly due to CO_2-induced warming (Fig. 1a). In the 1xDGVM experiment, GDD (i.e., annual growing degree days above 5 °C), which measures the accumulation of growing season warmth in a year, is largely less than 350 °C day at high latitudes inhibiting tree growth (Table 1) and the minimum monthly temperature is lower than −17 °C prohibiting grass growth (Table 1). In contrast, in the high CO_2 experiments, GDD is generally greater than 1200 °C day except in the cold Siberian interior due to the large increase in surface temperature (Fig. 1a), providing a sufficient growing season for all tree PFTs to thrive (Table 1). In addition, the minimum monthly temperature exceeds −17 °C, allowing the establishment of temperate trees and grasses. The retreat of subtropical grasses in the Southern Hemisphere in the two high CO_2 experiments is caused by a decrease in precipitation associated with enhanced subtropical subsidence. The decrease in low-latitude evergreen tree cover and increase in deciduous tree cover with higher

CO_2 are also associated with the decrease in precipitation (Fig. 1b).

The poleward expansion of trees at mid-to-high latitudes under high atmospheric CO_2 matches the fossil data reasonably well (Fig. 3). The simulated dominant woody PFTs at mid- and high-latitude North America, Greenland, coastal Eurasia, New Zealand, Australia and coastal Antarctica are supported by fossil woods and coal deposits (Beerling et al., 1999; Falcon-Lang et al., 2001; Herman and Spicer, 1996; Price et al., 1997). In contrast, the simulated predominant woody PFTs in the tropical South America and Africa appears inconsistent with the presence of fossil elaterate assemblages, a unique palynoflora assemblage indicating arid climate (Dino et al., 1999). The dense tropical trees simulated in our model are similar to the simulated mid-Cretaceous vegetation pattern by the University of Sheffield dynamic global vegetation model or FOAM-LPJ (Beerling et al., 1999; Donnadieu et al., 2009).
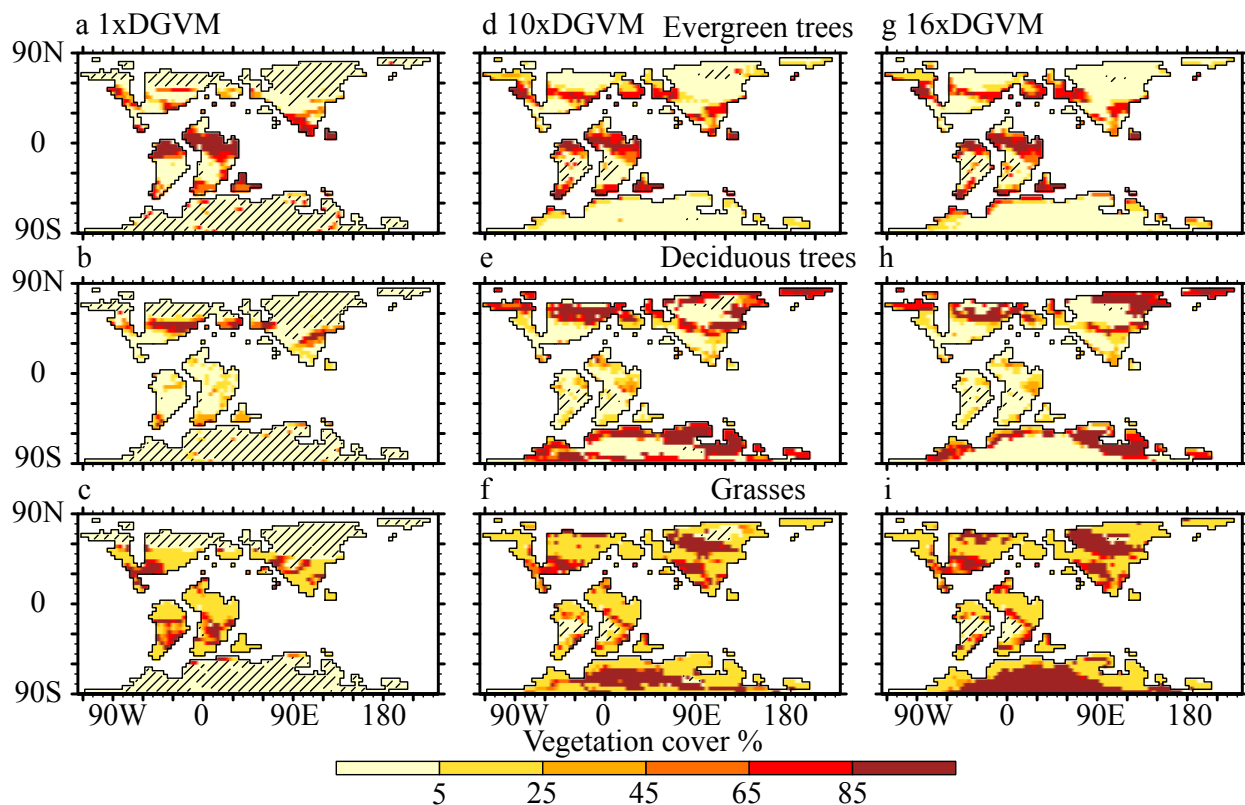
Fig. 2. Global distribution of evergreen trees **(a)**, **(d)**, **(g)**, deciduous trees **(b)**, **(e)**, **(h)** and grasses **(c)**, **(f)**, **(i)** (%) for the 1xDGVM, 10xDGVM, and 16xDGVM experiments, respectively. Land area with <10 % vegetation cover, which is defined as desert, is shaded. Note, hereafter, continental outlines delimit area with >50 % land cover. Evergreen trees include tropical and temperate broadleaf evergreen, and temperate and boreal needleleaf evergreen. Deciduous trees include tropical and temperate broadleaf deciduous and boreal deciduous.

3.2 Impact of vegetation on mid-Cretaceous climate

3.2.1 Land surface response

The presence of vegetation in the 10xDGVM experiment increases mid-Cretaceous global surface temperature by 0.9 °C (Table 2). Changes in surface temperature show significant spatial (Fig. 4b) and seasonal variations (Fig. 5a, f and k). High-latitude forested areas experience annual warming of 2.3 °C with early summer warming of up to 4.0 °C (Figs. 4b and 5a). In contrast, low-latitude forested areas undergo year-round cooling (Figs. 4b and 5f). Mid-latitude Northern Hemisphere surface temperatures increase during the cold seasons and decrease during the warm seasons (Fig. 5k). Changes in surface temperatures over ocean are generally less than 1 °C at low latitudes and up to 3 °C at high latitudes (Fig. 4b). The maximum increase in surface temperature (>5 °C) occurs in the mid-latitude North Pacific, and is caused by the poleward shift of western boundary currents (explained in Sect. 3.2.3).

The changes in land surface temperature can be explained by the net effect of vegetation-induced changes in latent heat fluxes and surface absorbed solar radiation. The former results from changes in evapotranspiration (Fig. 6a); the latter is mainly due to changes in surface albedo (Fig. 6b) and low-cloud cover (Fig. 6c). As a result of canopy evapotranspiration, the total annual mean evapotranspiration over land increases by 0.38 mm day^{-1} (22.7 %) in the 10xDGVM experiment relative to the 10xBG experiment (Fig. 6a). And the increase (>1.0 mm day^{-1}) is most significant over the low-to-mid latitude evergreen forests. In contrast, the annual mean land surface albedo decreases by 0.04 (~20 %) in the 10xDGVM experiment (Fig. 6b and Table 3), due to the darkening of land surface via forests, and to a less extent via reduced snow cover. The reduction (up to 0.2) is most pronounced over mid-to-high latitude deciduous forests through snow-masking (Fig. 6b). Seasonally, over high-latitude forests, the net surface radiation (i.e., the difference between surface absorbed solar radiation and net upward longwave radiation) increases by ~24 W m^{-2} due to the large gain in surface absorbed solar radiation (>31 W m^{-2}) during late spring and early summer (Fig. 5c), which greatly exceeds increases in latent heat fluxes (Fig. 5b), leading to significant warming (Fig. 5a). The increases in surface absorbed solar radiation are due to (1) decreases in surface

Table 3. Global and high-latitude annual mean climatic variables in the 10xBG and 10xDGVM experiments.

Variable/Experiment	10xBG	10xDGVM	10xDGVM-10xBG
SAT (land, 60–90° N, °C)	4.4	6.3	1.9
SAT (ocean, 60–90° N, °C)	8.1	10.0	1.9
SAT (land, 60–90° S, °C)	4.7	6.4	1.7
SAT (ocean, 60–90° S, °C)	11.0	12.3	1.3
Snow fraction (land, 60–90° N)	0.12	0.09	−0.03
Snow fraction (land, 60–90° S)	0.14	0.10	−0.04
Polar sea ice fraction	0.005	0.002	−0.003
Surface albedo (land)	0.203	0.163	−0.04
Surface albedo (land, 60–90° N)	0.273	0.216	−0.057
Surface albedo (land, 60–90° S)	0.304	0.242	−0.062
Surface LW↓ (ocean, $W m^{-2}$)	396.7	404.0	7.3
Latent heat fluxes↑ ($W m^{-2}$)	97.1	100.5	3.4
Latent heat fluxes↑ (land, $W m^{-2}$)	48.8	59.9	11.1
Precipitable water ($kg m^{-2}$)	37.8	41.1	3.3
Precipitation (land, $mm day^{-1}$)	2.69	2.95	0.26
Snow (land, $mm day^{-1}$)	0.12	0.10	−0.02
Precipitation (ocean, $mm day^{-1}$)	3.57	3.64	0.07
Evapotranspiration (land, $mm day^{-1}$)	1.69	2.07	0.38
MOC (Northern Hemisphere, Sv)	21.4	16.9	−4.5
MOC (Southern Hemisphere, Sv)	9.3	8.3	−1.0
OHT (Northern Hemisphere, PW)	1.84	1.61	−0.23
OHT (Southern Hemisphere, PW)	1.16	1.09	−0.07

Fig. 3. Distribution of mid-Cretaceous vegetation inferred from fossil wood, pollen of Elaterate assemblages and coal deposits and comparison with simulated vegetation. Fossil wood (solid circle) and coal deposits (solid star) are indicators of high-productivity forests; fossil pollen of Elaterates assemblages (down triangle) indicates dry climate and/or mangrove swamps and savannah (Dino et al., 1999; Ziegler et al., 2003). Paleofloral data is adapted from Beerling et al. (1999), Dino et al. (1999), Falcon-Lang et al. (2001), Herman and Spicer (1996) and Price et al. (1997). The shading of symbols shows agreement between the simulated vegetation in the 10xDGVM experiment and paleofaunal data. Black indicates that the model simulates the observed faunal type; red indicates that it does not. The model-data comparison (not shown) is nearly identical for the 16xDGVM experiment.

reflected solar radiation associated with the reduction in surface albedo (Fig. 5d), and (2) increases in incoming solar radiation associated with reduced low cloud cover (Fig. 6c). The decreases in low cloud cover are linked to the reduced boundary layer relative humidity with increased temperatures. In contrast, over low-latitude forests, increases in latent heat fluxes are up to 31 (26) $W m^{-2}$ greater than increases in surface absorbed solar radiation in the Northern (Southern) Hemisphere (Fig. 5g and h) leading to significant cooling (Fig. 5f). The increases in absorbed solar radiation are significantly smaller than the surface albedo feedback (Fig. 5i), because low-latitude forest evapotranspiration leads to denser low cloud cover (Fig. 6c) and, thus, offsets the surface albedo feedback by reducing incoming solar radiation at the surface (Fig. 5j). Over the northern mid-latitude forests, the increases in latent heat fluxes are up to 35 $W m^{-2}$ greater than increases in absorbed solar radiation during summer (Fig. 5l and m) leading to summer cooling (Fig. 5k).

Unlike over land, changes in surface albedo are negligible over ocean except the northern Eurasian coastal area (Table 3 and Fig. 6b). The large-scale background warming over ocean results from the increase in downwelling longwave radiation (7.3 $W m^{-2}$) (Table 3) associated with elevated atmospheric water vapour content (correlation > 0.7). Warming over the southern South Atlantic and Tethys Ocean, the equatorial and northern mid-latitude Pacific Ocean, and the Western Interior Seaway is also enhanced by positive cloud
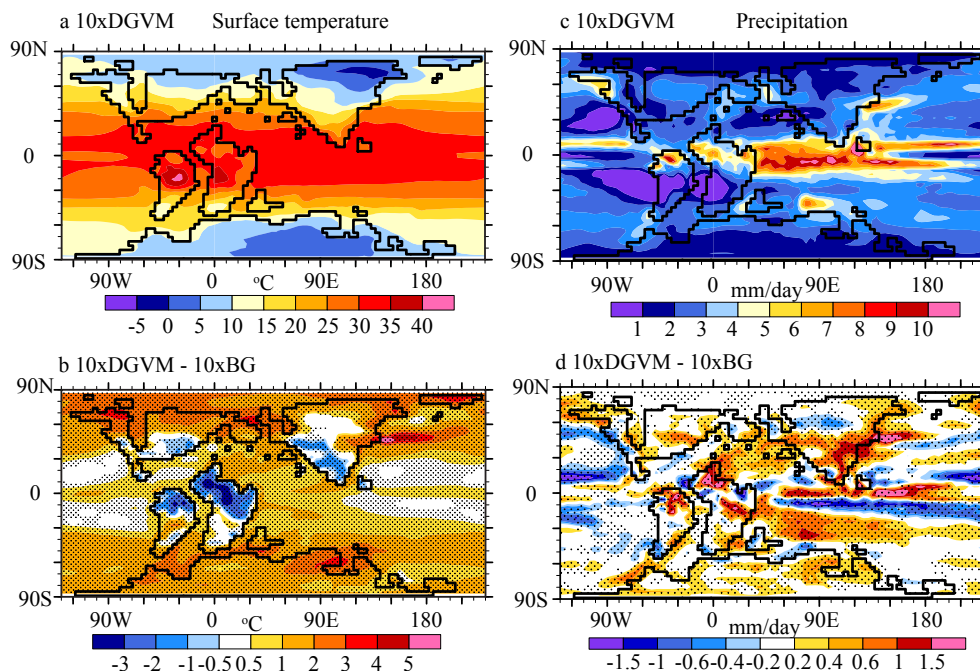
Fig. 4. Mean annual surface temperature (°C) and precipitation (mm day^{-1}) for (**a, c**) 10xDGVM experiment; and (**b, d**) 10xDGVM–10xBG experiments. In (**b, d**), the differences exceed 95 % confidence level are shaded.

radiative forcing due to reduced low cloud cover (Fig. 6c). In contrast, warming over the subtropical Pacific Ocean is suppressed by negative cloud radiative forcing due to increased low cloud cover.

3.2.2 Precipitation response

From a global perspective, the presence of vegetation slightly intensifies the mid-Cretaceous hydrological cycle (Table 3). As a result of the increases in the surface temperature and evapotranspiration, the global precipitable water (i.e., vertically integrated specific humidity) and precipitation increases by 3.3 kg m^{-2} (8.7 %) and 0.11 mm day^{-1} (3.3 %), respectively. In contrast, snowfall decreases by 0.02 mm day^{-1} (17 %) over land. The increases in precipitation are more pronounced over land (0.26 mm day^{-1}, 9.7 %) than over ocean (0.07 mm day^{-1}, 2.0 %). Due to enhanced precipitation, the freshwater flux into the high-latitude North and South Pacific Ocean increases by 0.05 Sv (15.2 %) and 0.03 Sv (11.5 %), respectively.

The presence of vegetation leads to significant regional changes in precipitation, though the large-scale precipitation pattern remains unchanged (Fig. 4d). The most significant regional changes (>1.0 mm day^{-1}) occur over the low-to-mid latitude forests, intertropical convergence zones (ITCZ) and mid-latitude Western Pacific. The increases in continental precipitation are mainly due to the enhanced recycling of water via canopy evapotranspiration, with a point-to-point correlation larger than 0.6 over most areas.

In contrast, the changes in precipitation over ocean mainly reflect changes in large-scale atmospheric circulation, as shown by the changes in zonal-average annual mean meridional streamfunction (Fig. 7a). The Hadley cells weaken by 3.2×10^9 kg s^{-1} (3 %) and 6.3×10^9 kg s^{-1} (7 %) in the Northern and Southern Hemisphere, respectively, due to the reduced equator-to-pole temperature gradient. In addition, the ascending branches of the Hadley cells contract equatorward (from ~16.7° N/S to 13.0° N/S). The equatorward contraction in each hemisphere mainly occurs during winter and spring seasons when the Hadley cell expands to the other hemisphere (not shown). The weakening and contraction of Hadley cells cause anomalous ascending motion at equatorial latitudes (~5° S–5° N) and ~20–40° N/° S and anomalous subsidence at ~10–20° N/° S. As a result, precipitation increases at ~5° S–5° N and 20–40° N/° S and decreases at ~10–20° N/° S. The increase in precipitation at mid-latitude North Pacific is associated with warming due to a poleward shift of the western boundary currents.

3.2.3 Ocean circulation response

The reduction in the equator-to-pole temperature gradient in the 10xDGVM experiment leads to a decrease in zonal wind strength. As shown in Fig. 7b, the maximum zonal-mean wind stress over the Pacific Ocean decreases by 0.02 N m^{-2} (~13 %) in the Southern Hemisphere and 0.03 N m^{-2} (~20 %) in the Northern Hemisphere. As a result, the maximum intensity of the subtropical gyres
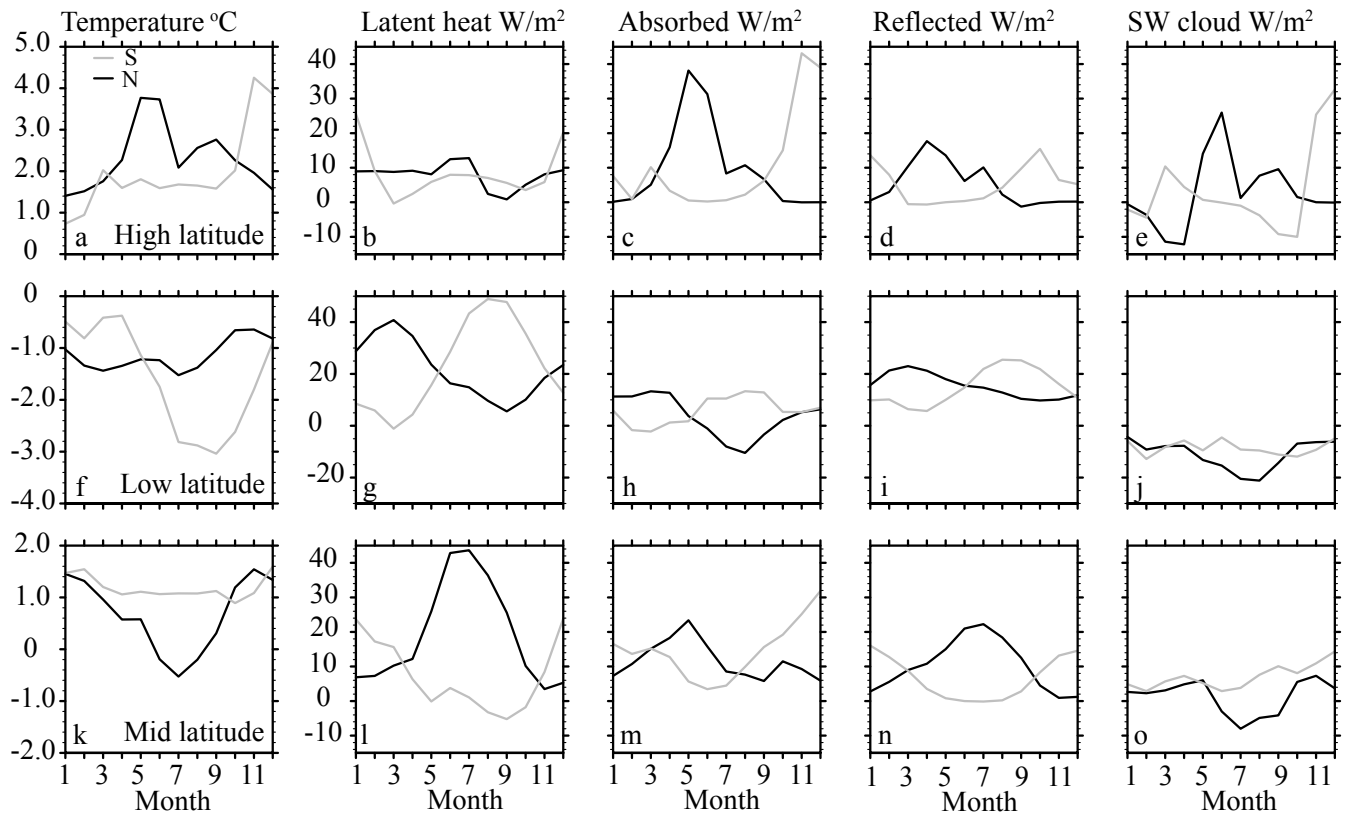
Fig. 5. Annual cycles of surface temperature (°C), latent heat fluxes (W m^{-2}), surface absorbed solar radiation (W m^{-2}), surface reflected solar radiation (W m^{-2}), surface shortwave cloud forcing (W m^{-2}) over the high-latitude forests **(a–e)**, low-latitude forests **(f–j)** and mid-latitude forests **(k–o)** for 10xDGVM–10xBG experiments. Solid black lines denote changes in the Northern Hemisphere and grey lines denote changes in the Southern Hemisphere. Low, mid and high latitudes are defined as 30° S–30° N, 30–50° S/° N and 60–90° S/° N, respectively.

decreases by 7.9 Sv (10 %) from 77.1 Sv (10xBG) to 69.2 Sv (10xDGVM) in the Northern Hemisphere and by 14.0 Sv (13.3 %) from 105.4 Sv (10xBG) to 91.4 Sv (10xDGVM) in the Southern Hemisphere. In addition, the mean position of the maximum wind stress shifts poleward by a grid cell (3.75°) from 50.1° N to 53.8° N in the Northern Hemisphere. Consistent with this poleward shift in wind stress, the western boundary current shifts from ~43° N in the 10xBG experiment to ~46° N in the 10xDGVM experiment in the western North Pacific. This poleward displacement of warm, saline subtropical water leads to the significant increase in temperature (>5 °C) (Fig. 4b) and salinity (>2 PSU) at ~45° N.

Vegetation also weakens the intensity of global MOC, though the pattern of MOC remains the same (with deep water mainly formed in the northern Pacific Ocean). As shown in Fig. 8, the maximum magnitude of MOC decreases by 1.0 Sv (~11 %) from 9.3 Sv in the 10xBG experiment to 8.3 Sv in the 10xDGVM experiment in the Southern hemisphere and decreases by 4.5 Sv (~21 %) from 21.4 Sv in the 10xBG experiment to 16.9 Sv in the 10xDGVM exper-

iment in the Northern hemisphere. This decrease is 0.8 Sv larger than CO$_2$-induced decrease between the 10xDGVM and 1xDGVM (20.6 Sv) experiments. The slight weakening of MOC in the Southern Hemisphere is caused by warming (Fig. 4b) and freshening through enhanced precipitation (Fig. 4d) of the high-latitude South Pacific. In addition to the freshening via enhanced precipitation, the poleward migration of the low-salinity subpolar front associated with the poleward shift of the western boundary currents, also contributes to the decrease in seawater salinity at the high-latitude North Pacific. As a result, deep water formation along the Northeast coast of Asia vanishes and MOC slows down in the Northern Hemisphere. In response to the weakening of MOC, poleward oceanic heat transport decreases by 0.07 PW (~6 %) in the Southern Hemisphere and 0.23 PW (~13 %) in the Northern Hemisphere (Table 3). This decrease in poleward heat transport diminishes the warming over the high-latitude Pacific Ocean (~70° S/° N) (Fig. 4b).
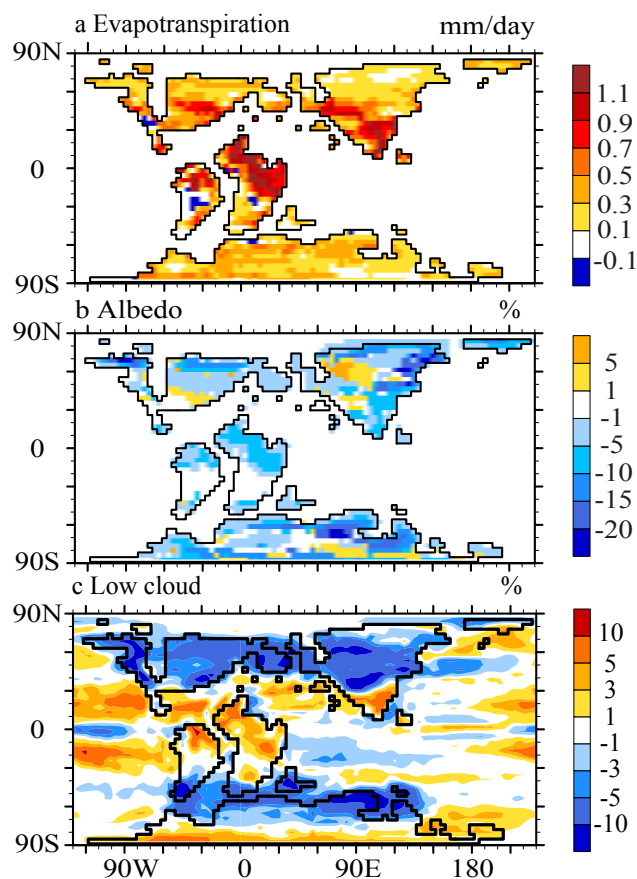
Fig. 6. Annual mean **(a)** total evapotranspiration over land (mm day^{-1}); **(b)** surface albedo (%); and **(c)** low cloud cover (%) for the 10xDGVM–10xBG experiments (%).

4 Discussion

4.1 The role of vegetation feedbacks under high CO_2

Our results show that vegetation acts to warm high latitudes and cool low latitudes in a warm climate with high CO_2, similar to the role of modern vegetation (Bonan, 2008). The simulated warming effect of high-latitude forests on polar regions is also consistent with previous Cretaceous studies (Deconto et al., 2000; Otto-Bliesner and Upchurch, 1997; Upchurch et al., 1998). However, our simulated reduction in high-latitude surface albedo ($\sim$0.06) and the associated warming ($<2\,°C$) are more than one-half less than in these studies, mainly because we assess the impact of vegetation in a warm mean climate with little snow (<0.15) and sea ice (<0.01) (Table 3). In contrast, using a atmospheric CO_2 value of 580 ppmv, Upchurch et al. (1998) report that snow and sea ice fraction are up to 0.62 and 0.38, allowing a stronger vegetation-snow-sea ice albedo feedback. The weaker warming here is also linked to the decrease in poleward oceanic heat transport resulting from the weakening of MOC, which is not resolved in the earlier studies. The simulated mean annual temperatures over the Eurasian inte-

rior and Arctic Ocean only increase $\sim$2 °C by vegetation and are up to 10 °C lower than those estimated by proxies such as leaf physiognomy (Spicer et al., 2002, 2008) and TEX$_{86}$ method (Jenkyns et al., 2004). Moreover, as the vegetation-induced warming is most pronounced during the warm late spring-early summer (Fig. 5a), the inclusion of vegetation does not help to reduce high-latitude seasonality. Therefore, we conclude that high-latitude forests can only be considered a secondary mechanism for the mid-Cretaceous polar warmth. Other mechanisms in addition to high atmospheric CO_2 and high-latitude vegetation are required to maintain the polar warmth.

We find that $\sim$20–40 % of the increase in surface absorbed solar radiation over high-latitude forests is due to cloud feedbacks. In fact, the increase in cloud radiative forcing surpasses the albedo feedback during late spring and early summer (Fig. 5d, e). This positive cloud feedback contradicts a previous study (Betts, 1999), which reports that the presence of vegetation induced a high-latitude summer cooling of $>2\,°C$ mainly by reducing surface solar radiation via enhanced cloud cover. These contrasting results highlight the uncertainty of cloud feedbacks in determining the overall effect of high-latitude forests.

4.2 Oceanic circulation

Our simulations are consistent with modelling studies with a dynamic ocean component that vegetation can have an important impact on MOC, due to vegetation-induced changes in hydrological cycle and sea surface temperature (Brovkin et al., 2002, 2009; Ganopolski et al., 1998; Lohmann et al., 2006). Moreover, our simulations suggest that the response of MOC to vegetation could exceed that of a tenfold increase in atmospheric CO_2 concentration. Proxy records and model studies demonstrate that global vegetation pattern is highly correlated with climate changes during the geological past and future (e.g., Spicer and Chapman, 1990; Alo and Wang, 2008; Cramer et al., 2001). Therefore, vegetation-climate interactions should be taken into account for simulating the MOC response to past and future climate change.

5 Caveats

In the absence of global paleovegetation reconstructions, most previous modelling studies of the mid-Cretaceous have assumed a uniform vegetation type on all continents (e.g., Donnadieu et al., 2006; Poulsen et al., 2007; Zhou et al., 2008). In this contribution, we use a dynamic vegetation model to overcome this limitation. We emphasise, though, that the simulation of pre-Quaternary vegetation is subject to uncertainty, mainly due to a paucity of evidence for the construction and physiology of past ecosystems. Due to our lack of understanding of past ecosystems, paleovegetaion modelling relies on a modern understanding of PFTs and their bioclimatic, physiological and dynamic relationships that may not be entirely appropriate for past times. For
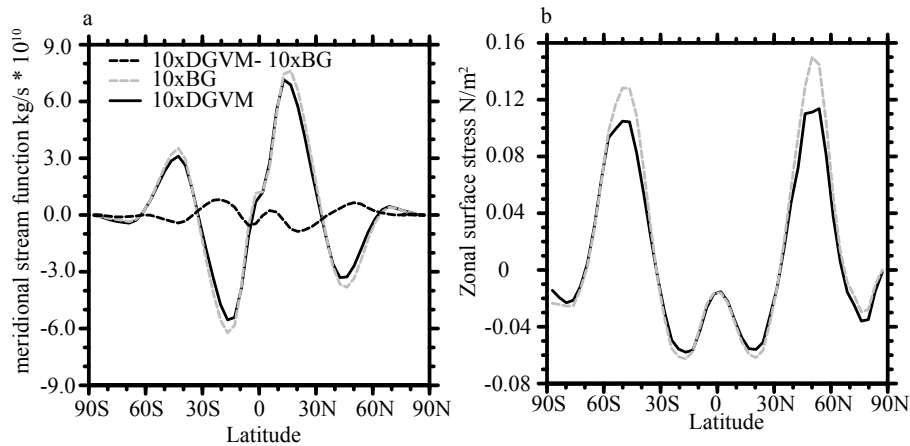
Fig. 7. Zonal-average annual mean meridional streamfunction (10^{10} kg s^{-1}) at 400 mb **(a)**; and wind stress (N m^{-2}) over the Pacific Ocean **(b)** for the 10xDGVM (black solid line), 10xBG (grey dashed line) and 10xDGVM–10xBG experiments (black dashed line), respectively.
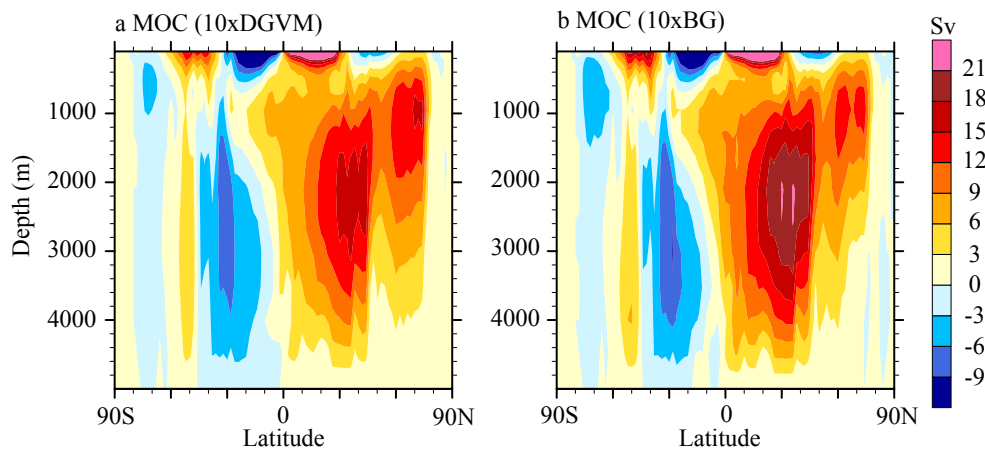

Fig. 8. Annual mean Meridional overturning circulation (Sv) for **(a)** 10xDGVM experiment; and **(b)** 10xBG experiment. Positive (in yellow and red) means clockwise flow direction and negative means counterclockwise flow direction.

example, grass, which is a dominant PFT at present, had not evolved in mid-Cretaceous. We keep grass in our simulation because it is the only available herbaceous PFT. Another substantial change between the modern and mid-Cretaceous is angiosperms. The modern angiosperm-dominated tropical forests may not have appeared until the Paleocene (Burnham and Johnson, 2004). Yet our simulations show extensive tropical forests resembling the modern distribution, an overestimation that may be linked to the inclusion of PFTs that represent modern angiosperm trees. Consequently, CLM-DVGM may overestimate the impact of low-latitude vegetation on mid-Cretaceous climate, because angiosperms have a much larger impact on hydrology relative to other plants due to their high transpiration capacity (Boyce and Lee, 2010). Another uncertainty in our simulations is the use of modern physiological pCO$_2$ (355 ppmv). Presumably, increasing atmospheric pCO$_2$ could enhance plant growth and reduce plant transpiration. As a result, our model might un-

derestimate vegetation productivity and overestimate canopy evapotranspiration. To more accurately simulate the mid-Cretaceous vegetation and its feedbacks, more paleovegetation data is needed to appropriately parameterize the mid-Cretaceous dominant PFTs.

6 Conclusions

We investigate the vegetation-climate interaction using a coupled ocean-atmosphere GCM (CCSM3) with a dynamic vegetation component. The model demonstrates a positive feedback between vegetation and polar climate; CO$_2$-induced warming promotes expansion of high-latitude forests, which leads to additional polar warming via reducing surface albedo and low cloud cover. However, the warming effect of vegetation at high latitudes is smaller than reported in previous studies, mainly due to the less pronounced surface albedo feedback in the absence of large snow and sea

ice cover under the simulated warm mean climate. Over low latitude continents, the feedbacks between vegetation and climate are opposite; forest cover decreases with higher CO_2, and the presence of forests leads to year-round cooling. The cooling is associated with enhanced evapotranspiration and low cloud cover.

The simulation of mid-Cretaceous vegetation has unexpected effects on the ocean. First, as a result of the enhanced atmospheric vapour content with vegetation, downwelling longwave radiation increases over ocean, leading to surface warming at sea surface. Second, vegetation alters wind fields, resulting in weakening of wind-driven subtropical and subpolar gyres and poleward displacement of the North Pacific western boundary current. Lastly, the intensified precipitation enhances the freshwater flux into the high-latitude Pacific. This freshening in conjunction with surface warming reduces the meridional overturning circulation in both hemispheres, which reduces meridional heat transport and damps high-latitude warming.

References

Abbot, D. S. and Tziperman, E.: A high-latitude convective cloud feedback and equable climates, Q. J. Roy. Meteorol. Soc., 134, 165–185, 2008.

Alo, C. A. and Wang, G.: Potential future changes of the terrestrial ecosystem based on climate projections by eight general circulation models, Geophys. Res. Lett., 113, G01004, doi:10.1029/2007JG000528, 2008.

Barron, E. J.: Cretaceous plate tectonic reconstructions, Palaeogeogr., Palaeocl., 59, 3–29, 1987.

Barron, E. J. and Washington, W. M.: Warm Cretaceous climates: High atmospheric CO_2 as a plausible mechanism, in: The carbon cycle and atmospheric CO_2: Natural variations, edited by: Sundquist, E. T. and Broecker, W. S.: Archean to present, American Geophysical Union Geophysical Monograph, 32, 546–553, 1985.

Barron, E. J., Fawcett, P. J., Peterson, W. H., Pollard, D., and Thompson, S. L.: A "simulation" of Mid-Cretaceous climate, Paleoceanography, 10, 953–962, 1995.

Beerling, D. J., Woodward, F. I., and Valdes, P. J.: Global terrestrial productivity in the mid-Cretaceous (100Ma): Model simulations and data, in: Evolution of the Cretaceous ocean-climate system, edited by: Barrera, E. and Johnson, C., Spec. Pap. Geol. Soc. Am., 332, 385–390, 1999.

Betts, R. A.: Self-beneficial effects of vegetation on climate in an ocean-atmosphere general circulation model, Geophys. Res. Lett., 26, 1457–1460, 1999.

Bice, K. L. and Norris, R. D.: Possible atmospheric CO_2 extremes of the Middle Cretaceous (late Albian-Turonian), Paleoceanography, 17, 1070, doi:10.1029/2002PA000778, 2002.

Bice, K. L., Huber, B. T., and Norris, R. D.: Extreme polar warmth during the Cretaceous greenhouse? Paradox of the late Turonian $\delta^{18}O$ record at Deep Sea Drilling Project Site 511, Paleoceanography, 18, 1031, doi:10.1029/2002PA000848, 2003.

Bice, K. L., Birgel, D., Meyers, P. A., Dahl, K. A., Hinrichs, K., and Norris, R. D.: A multiple proxy and model study of Cretaceous upper ocean temperatures and atmospheric CO_2 concentrations, Paleoceanography, 21, PA2002, doi:10.1029/2005PA001203, 2006.

Bonan, G. B.: Forests an climate change: forcings, feebacks, and the climate benefits of forests, Science, 320, 1444–1449, 2008.

Bonan, G. and Levis, S.: Evaluating aspects of the Community Land and Atmosphere Models (CLM3 and CAM3) using a dynamic global vegetation model, J. Climate, 19, 2290–2301, 2006.

Bonan, G. B., Levis, S., Sitch, S., Vertenstein, M., and Oleson, K.: A dynamic global vegetation model for use with climate models: concepts and description of simulated vegetation dynamics, Glob. Change Biol., 9, 1543–1566, 2003.

Boyce, C. K. and Lee, J. E.: An exceptional role for flowering plant physiology in the expansion of tropical rainforests and biodiversity, Proc. Roy. Soc. Lond., Ser. B, Biol. Sci., 277, 3437–3443, 2010.

Branstetter, M. L.: Development of a parallel river transport algorithm and applications to climate studies, Ph.D. thesis, University of Texas at Austin, 119 pp., 2001.

Brovkin, V.: Climate-vegetation interaction, J. Phys. IV FRANCE, 12, 10–57, 2002.

Brovkin, V., Raddatz, T., Reich, C. H., Claussen, M., and Gayler, V.: Global biogeophysical interactions between forest and climate, Geophys. Res. Lett., 36, L07405, doi:10.1029/2009GL037543, 2009.

Burnham, R. J. and Johnson, K. R.: South American palaeobotany and the origins of neotropical rainforests, Phil. Trans. R. Soc. Lond. B, 359, 1595–1610, 2004.

Cerling, T. E., Wang, Y., and Quade, J.: Expansion of C_4 ecosystems as an indicator of global ecological change in late Miocene, Nature, 361, 344–345, 1993.

Collins, W. D., Bitz, C. M., Blackmon, M. L., Bonan, G. B., Bretherton, C. S., Carton, J. A., Chang, P., Doney, S. C., Hack, J. J., Henderson, T. B., Kiehl, J. T., Large, W. G., McKenna, D. S., Santer, B. D., and Smith, R. D.: The Community Climate System Model Version 3 (CCSM3), J. Climate, 19, 2122–2143, 2006.

Covey, C. and Barron, E.: The role of ocean heat transport in climatic change, Earth-Sci. Rev., 21, 429–445, 1988.

Cramer, W., Bondeau, A., Woodward, F. I., Prentice, I. C., Betts, R. A., Brovkin, V., Cox, P., Fisher, V., Foley, J. A., Friend, A. D., Kucharik, C., Lomas, M., Ramankutty, N., Sitch, S., Smith, B., White, A., and Young-Molling, C.: Global response of terrestrial ecosystem structure and function to CO_2 and climate change: results from six dynamic global vegetation models, Glob. Change Biol., 7, 357–373, 2001.

Donnadieu, Y., Pierrehumbert, R., Jacob, R., and Fluteau, F.: Modelling the primary control of paleogeography on Cretaceous climate, Earth Planet. Sci. Lett., 248, 426–437, 2006.

Donnadieu, Y., Goddéris, Y., and Bouttes, N.: Exploring the climatic impact of the continental vegetation on the Mezosoic

atmospheric CO_2 and climate history, Clim. Past, 5, 85–96, doi:10.5194/cp-5-85-2009, 2009.

DeConto, R. M., Brady, E. C., Bergengren, J., and Hay, H. H.: Late Cretaceous Climate, Vegetation, and Ocean Interactions, in: Warm Climates in Earth History, edited by: Huber, B., MacLeod, K. G., and Wing, S. L., Cambridge University Press, 275–297, 2000.

Dino, R., Pocknall, D. T., and Dettmann, M. E.: Morphology and ultrastructure of elater-bearing pollen from the Albian to Cenomanian of Brazil and Ecuador: implications for botanical affinity, Rev. Palaeobot. Palyno., 105, 201–235, 1999.

Farrel, G. F.: Equable climate dynamics, J. Atmos. Sci., 47, 2986–2995, 1990.

Falcon-Lang, H. J., Cantrill, D. J., and Nichols, G. J.: Biodiversity and terrestrial ecology of a mid-Cretaceous, high-latitude floodplain, Alexander Island, Antarctica, J. Geol. Soc., 158, 709–724, 2001.

Ganopolski, A., Kubatzki, C., Claussen, M., Brovkin, V., and Petoukhov, V.: The influence of vegetation-atmosphere-ocean interaction on climate during the mid-Holocene, Science, 280, 1916–1919, 1998.

Gough, D. O.: Solar interior structure and luminosity variations, Sol. Phys., 74, 21–34, 1981.

Herman, A. B. and Spicer, R. A.: Palaeobotanical evidence for a warm Cretaceous Arctic Ocean, Nature, 380, 330–333, 1996.

Jacobs, B. F., Kingston, J. D., and Jacobs, L. L.: The origin of grass-dominanted ecosystems, Ann. Missouri Bot. GARD., 86, 590–643, 1999.

Jenkyns, H. C., Forster, A., Schouten, S., and Damsté, J. S. S.: High temperatures in the Late Cretaceous Arctic Ocean, Nature, 432, 888–892, 2004.

Kiehl, J. T. and Shields, C. A.: Climate simulation of the latest Permian: implications for mass extinction, Geology, 33, 757–760, 2005.

Körner, C.: Ecological impacts of atmospheric CO_2 enrichment on terrestrial ecosystems, Philos. T. Roy. Soc. Lond., 361, 2023–2041, 2003.

Korty, R. L., Emanuel, K. A., and Scott, A. J.: Tropical cyclone-induced upper-ocean mixing and climate: application to equable climate, J. Climate, 21, 638–654, 2008.

Kump, L. R. and Pollard, D.: Amplification of Cretaceous warmth by biological cloud feedbacks, Science, 320, 195, doi:10.1126/science.1153883, 2008.

Levis, S., Bonan, G. B., Vertenstein, M., and Oleson, K. W.: The Community Land Model's dynamic global vegetation model (CLM-DGVM): Technical description and user's guide, NCAR Tech. Note TN-459_IA, 50 pp., 2004.

Lohmann, G., Butzin, M., Micheels, A., Bickert, T., and Mosbrugger, V.: Effect of vegetation on the Late Miocene ocean circulation, Clim. Past Discuss., 2, 605–631, doi:10.5194/cpd-2-605-2006, 2006.

Otto-Bliesner, B. L. and Upchurch Jr., G. R.: Vegetation-induced warming of high-latitude regions during the Late Cretaceous period, Nature, 385, 804–807, 1997.

Otto-Bliesner, B. L., Brady, E. C., and Shields, C.: Late Cretaceous ocean: Coupled simulations with the National Center for Atmospheric Research Climate System Model, J. Geophys. Res., 107, 4019, doi:10.1029/2001JD000821, 2002.

Peng, C. H.: From static biogeographical model to dynamic global vegetation model: a global perspective on modelling vegetation dynamics, Ecol. Modell., 135, 33–54, 2000.

Price, G. D., Valdes, P. J., and Sellwood, B. W.: Quantitative palaeoclimate GCM validation: Late Jurassic and mid-Cretaceous case studies, J. Geol. Soc., 154, 769–772, 1997.

Poulsen, C. J.: A balmy Arctic, Nature, 432, 814–815, 2004.

Poulsen, C. J., Barron, E. J., and Peterson, W. H.: A reinterpretation of mid-Cretaceous shallow marine temperatures through model-data comparison, Paleoceanography, 14, 679–697, 1999.

Poulsen, C. J., Gendaszek, A. S., and Jacob, R. L.: Did the rifting of the Atlantic Ocean cause the Cretaceous thermal maximum? Geology, 31, 115–118, 2003.

Poulsen, C. J., Pollard, D., and White, T. S.: General circulation model simulation of the $\delta^{18}O$ content of continental precipitation in the middle Cretaceous: A model-proxy comparison, Geology, 35, 199–202, 2007.

Scotese, C. R.: Times of global plate tectonic reorganization and their causes [abs]: Earth system processes, Programmes with Abstracts: London, Geological Society of London and Geological Society of America, p. 102, 2001.

Schlesinger, W. H.: Biogeochemistry: An analysis of global change 2nd end, Academic Press, San Diego, 1997.

Sloan, L. C. and Pollard, D.: Polar Stratospheric clouds: A high latitude warming mechanism in an ancient greenhouse world, Geophys. Res. Lett., 25, 3517–3520, 1998.

Spicer, R. A. and Chapman, J. L.: Climate change and the evolution of high-latitude terrestrial vegetation and floras. TREE, 5, 279–284, 1990.

Spicer, R. A. and Parrish, J. T.: Paleobotanical evidence for cool north polar climates in middle Cretaceous (Albian-Cenomanian) time, Geology, 14, 703–706, 1986.

Spicer, R. A., Rees, P. M., and Chapman, J. L.: Cretaceous phytogeography and climate signals, Philos. T. Roy. Soc. B, 341, 277–286, 1993.

Spicer, R. A., Ahlberg, A., Herman, A. B., Kelley, S. P., Raikevich, M. I., and Rees, P. M.: Palaeoenvironment and ecology of the middle Cretaceous Grebenka flora of northeastern Asia, Palaeogeogr. Palaeocl., 184, 65–105, 2002.

Spicer, R. A., Ahlberg, A., Herman, A. B., Hofmann, C., Raikevich, M., Valdes, P. J. and Markwich, P., J.: The Late Cretaceous continental interior of Siberia: a challenge for climate models, Earth Planet. Sci. Lett., 267, 228–235, 2008.

Upchurch Jr., G. R., Otto-Bliesner, B. L., and Scotese, C.: Vegetation-atmosphere interactions and their role in global warming during the latest Cretaceous, Philos. T. Roy. Soc. B, 353, 97–112, 1998.

Yeager, S. G., Shields, C. A., Large, W. G., and Hack, J. J.: The low-resolution CCSM3, J. Climate, 19, 2545–2566, 2006.

Ziegler, A. M., Eshel, G., Rees, P. M., Rothfus, T. A., Rowley, D. B., and Sunderlin, D.: Tracing the tropics across land and sea: Permian to present, Lethaia, 36, 227–254, 2003.

Zhou, J., Poulsen, C. J., Pollard, D., and White, T. S.: Simulation of modern and middle Cretaceous marine $\delta^{18}O$ with an ocean-atmosphere general circulation model, Paleoceanography, 23, PA3223, doi:10.1029/2008PA001596, 2008.